8-1-1973

Hot electron injection into dense argon, nitrogen, and hydrogen

Pavel Smejtek
Portland State University

M. Silver

K. S. Dy

David G. Onn

Citation Details

P. Smejtek, M. Silver, K. S. Dy, and D. G. Onn. Hot electron injection into dense argon, nitrogen, and hydrogen . J. Chem. Phys., 59:1374--1384, 1973.

Hot electron injection into dense argon, nitrogen, and hydrogen*

P. Smejtek,† M. Silver, and K. S. Dy
University of North Carolina, Chapel Hill, North Carolina 27514

D. G. Onn
University of Delaware, Newark, Delaware 19711

(Received 5 October 1972)

Hot electrons have been injected into very dense argon, nitrogen, and hydrogen gases and liquids. The current–voltage characteristics are experimentally determined for densities (N) of argon, nitrogen, and hydrogen ranging from about 10^{20} to 10^{22} cm^{-3} and applied fields (E) ranging from about 10 to 10^4 V cm^{-1}. The argon data show a square root E/N dependence of the current. The nitrogen and hydrogen data show a complicated dependence of the current on E/N due to the rapid thermalization in the region of the image potential of the injected electrons through inelastic collision processes not present in argon. A hydrodynamic-two-fluid model is developed to analyze the nitrogen and hydrogen data. From the analysis of our data, we obtain the density dependence of the momentum exchange scattering cross section and the energy relaxation time for the injected hot electrons.

I. INTRODUCTION

The gas density in the range between 10^{20} and 10^{22} cm^{-3} is of great interest for the theory of electron states and electron transport in disordered systems. At low densities, below 10^{21} cm^{-3}, the electron mobility is determined essentially by the electron–single-molecule-scattering cross sections. However, in liquified and very dense gases a number of new processes are operative. It is now well established that in dense helium electrons are localized,[1] while in liquid argon electrons propagate as quasi-free particles with longer mean free paths than those evaluated from the electron–atom scattering lengths.[2] On the other hand electron mobilities were found to be low[3] (about 10^{-2} cm^2/Vsec) in liquid N_2 and H_2. There is good evidence for bubbles[4] in H_2 but as yet none for N_2; consequently, a clear picture covering different types of systems is not yet available. To help give some further insight into this problem, we have studied the behavior of hot electrons (1 eV) by measuring the injection currents as a function of density and applied electric field.

In this paper we present some experimental data on hot electron injection currents into argon, nitrogen, and hydrogen. The experiments performed involved injecting hot electrons into a dense medium and studying the current–voltage characteristics as a function of density. The source of electrons used was a tunnel cathode. A description of these cathodes and their operation may be found in a review article by Crowell and Sze[5] and details in a paper by Onn, Smejtek, and Silver.[5] Figure 1 shows schematically how the diode works. When a forward bias is applied, electrons from the base aluminum are able to pass through the oxide and enter the emitter metal. A fraction of the electrons injected into the emitter have enough forward momentum to overcome the barrier and enter the insulating medium. Typically, we can operate the diode such that about 5×10^{-9} amps can be injected into vacuum (under these conditions the emitter-base current is about 10^{-5} A). Only a fraction of this current can enter the medium because there are scattering processes which reflect some of the carriers. In Fig. 2 we show a schematic representation of the possible scattering processes along with the potential due to the applied and image fields. An injected electron may undergo only momentum exchange scattering and be returned to the cathode as depicted by process 1. It may undergo only momentum exchange scattering but not be back scattered, and therefore it will slowly lose energy by these elastic processes until it is thermalized beyond the maximum in the potential. This is depicted by process 2. If there are energy exchange collisions such as excitations of rotational or vibrational modes of the medium, an electron may be rapidly thermalized before the maximum in the potential, process 3, or after the maximum in the potential, process 4. In general scattering processes 1 and 3 give rise to reflected currents (j_1 and j_3) while processes 2 and 4 give rise to transmitted currents (j_2 and j_4). In our experiment, we measure the net yield of the current

$$Y=[j_0-(j_1+j_3)]/j_0=(j_2+j_4)/j_0\,, \tag{1}$$

where j_0 is the injected current at the cathode.

Since it is the distance from the emitter where the electron reaches its equilibrium with the electric field which mostly determines whether the electron will be collected or not, and since the thermalization is taking place within 10^{-10} sec or less, the injection experiment does not require

such extremely pure media as the drift velocity one. This means that a gas purity of the order of 20 ppm, as used in our experiment, is completely satisfactory.

In the next section we discuss two theoretical expressions for the yield, Y, which we shall use in the analysis of our data. Both expressions are approximate and the detailed examination of the errors are given in the appendices. In the last section, we present the experimental results and discuss their physical significance.

II. THEORETICAL MODELS

A. Argon

Since inelastic scattering processes in argon are negligible compared with the elastic process, the yield in argon will come mainly from process 2 as depicted in Fig. 2. Thus

$$Y = j_2/j_0 = j_2/(j_2 + j_1) . \tag{2}$$

The first calculation of j_2 and j_1 was due to J. J. Thomson.[6] Thomson assumed that near the cathode the injected electrons have a random velocity $\bar{v}_0$ given by thermal equilibrium with the gas and that the density of electrons in the gas is uniform and of average value $n = n_\infty$, n_∞ being the density far from the cathode. It follows from these assumptions that $j_2 = n_\infty e\bar{v}$ and $j_1 = n_\infty e\bar{v}_0/4$, where $\bar{v}$ is the drift velocity of the electrons. Thomson thus obtained

$$Y = 4\bar{v}/(4\bar{v} + \bar{v}_0) . \tag{3}$$

Theobald[7] and Loeb[8] found that Eq. (3) gives reasonable fit to experiments only if $\bar{v}_0$ is reinterpreted as the average velocity of emission. Bekiarian[9] improved the theory further by taking the return current to be

$$j_1 = (1 - r)n_p e\bar{v}_0/4 , \tag{4}$$

where n_p is the density of electrons near the cathode and the factor $(1 - r)$ is included to account for the reflection of electrons at the cathode, r being the reflection coefficient. Equation (4) can be derived by solving a Boltzmann equation assuming that the energy change between collisions is small compared with the electron energy. The validity condition for this approximation is, however, difficult to ascertain because it requires the exact solution of the Boltzmann equation. So far the only way of deriving the exact solution is by a Monte Carlo technique.[10-12] Such a calculation, however, requires a very large amount of computer time. One simplified approach was made by Young and Bradbury[13] who calculated the return current assuming only reflection of electrons in their first encounter with gas atoms or molecules. Their calculation is based on the observation that the probability, $R(x)$, for an electron at a distance x from the cathode to be returned is proportional to the return cone at x and given by

$$R(x) = \tfrac{1}{2}\{1 - [eEx/(\mathcal{E}_0 + eEx)]^{1/2}\} , \tag{5}$$

where $\mathcal{E}_0$ is the injection energy and E is the applied electric field. By defining a transmission

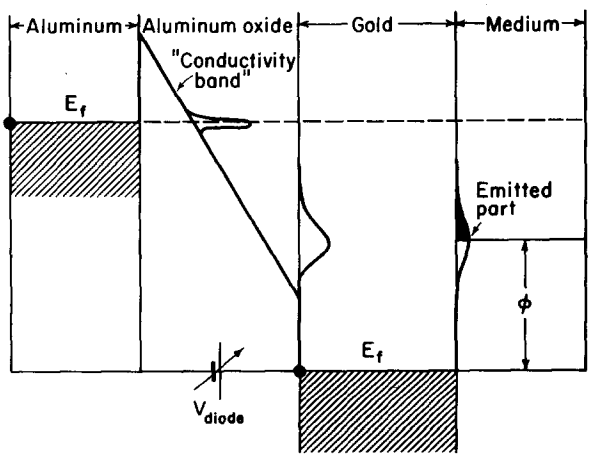

FIG. 1. Schematic diagram of the operation of a thin film MOM electron emitter. Under the applied bias V_{diode} electrons pass through the thin layer of Al_2O_3 into the thin gold electrode with extra kinetic energy. Only part of the electron distribution injected into the gold is finally emitted into the medium.

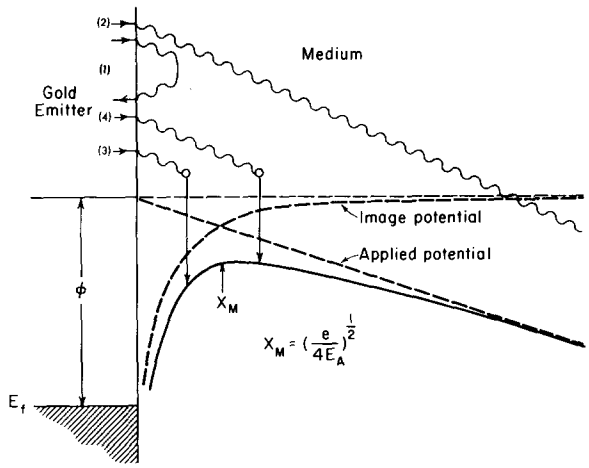

FIG. 2. Electrons emitted into the medium from the gold emitter are subjected to the following processes: (1) backscattering without a significant energy loss, (2) slow energy relaxation due to the elastic collisions only, (3) fast thermalization, the thermalization distance is shorter than the position of the maximum of the potential barrier x_M, the thermalized electrons have a large probability of being returned to the emitter, (4) fast thermalization, the thermalization distance is larger than x_M, the thermalized electrons have a large probability of being collected by the anode.

probability $T(x) \equiv 1 - R(x)$ we can rewrite Young and Bradbury's result in the following form, [14]

$$j_2 \approx j_0 \int_0^\infty dx\, N\sigma_p \exp(-N\sigma_p x)[T(x) - R(x)] , \qquad (6)$$

where σ_p is the momentum exchange scattering cross section and N is the density of particles. For $j_2/j_0 < 0.2$, the integral in (6) can be evaluated approximately to give

$$Y = j_2/j_0 \approx \tfrac{1}{2}\pi^{1/2}(eE\lambda/\mathcal{E}_0)^{1/2} , \qquad (7)$$

where $\lambda \equiv (N\sigma_p)^{-1}$ is the mean free path. Thus the Young and Bradbury assumptions predict a square root E/N dependence of the yield. From Eq. (6), it is obvious that Young and Bradbury's result becomes invalid when Thomson's assumptions hold because then $T(x) = R(x) = \frac{1}{2}$ and Eq. (6) gives $j_2 = 0$. It is difficult to assess when the Young and Bradbury's result becomes valid because a comparison with the exact solution of the Boltzmann equation would again be necessary. A plausible condition is that $T(\lambda)$ differ from $R(\lambda)$ by about 10%. From Eq. (5), we get

$$T(\lambda) - R(\lambda) = [eE\lambda/(\mathcal{E}_0 + eE\lambda)]^{1/2} > 0.1 . \qquad (8)$$

For the cases we shall be interested in, $eE\lambda \ll \mathcal{E}_0$, and Eq. (8) reduces to

$$eE\lambda/\mathcal{E}_0 > 0.01 . \qquad (9)$$

This condition is not significantly different from that found by Lucas[12] using a more precise Monte Carlo technique. For a gas of density $N \sim 10^{21}$ cm^{-3} and a scattering cross section $\sigma_p \sim 10^{-15}$ cm^2, typical of argon, Young and Bradbury's result would be valid for $E/N > 10^{-17}$ V · cm^2 if the injection energy $\mathcal{E}_0$ is taken to be 1 eV. It should be emphasized that the derivation of (6) requires several approximations which can not easily be justified. Application of the Monte Carlo technique should clarify most of the difficulties. We shall not attempt such a calculation here.

B. Nitrogen and Hydrogen

Since there are obviously inelastic rotational and vibrational modes which can be excited in both H_2 and N_2, all four types of scattering processes described in Fig. 2 will affect the current. The yield is given by

$$Y = (j_2 + j_4)/j_0 .$$

We shall be interested mainly in the region of small E/N ($eE\lambda/\mathcal{E}_0 < 0.01$) where the Boltzmann equation can be solved approximately by retaining only terms linear in the field and concentration gradient. However, because of the rapid energy relaxation processes ($\sim 10^{-10}$ sec or less) in nitrogen and hydrogen, the effect of the image potential becomes quite important and can not be neglected. As can be seen from Fig. 2, the magnitude of j_2 and j_4 depends on the position of the potential maximum x_M. At low fields, x_M is large and a large portion of the hot electrons will relax before reaching the potential maximum. At high fields, x_M is small and the majority of hot electrons will relax beyond x_M. In this way the image barrier probes the spatial distribution of the hot electrons. The inclusion of image field renders the solution of the Boltzmann equation quite difficult. We shall instead solve the hydrodynamic equations where an approximation we shall introduce can easily be made.

The electrons involved in the processes 2 and 4 depicted in Fig. 2 can be considered as a two-component fluid. We assume that one component of the fluid, the hot electrons with density ρ_h and current j_h, relaxes in an average time τ via the inelastic electron–medium interaction into the thermalized component with density ρ_t and current j_t. Because of the continuity of current, $\nabla \cdot (\vec{j}_h + \vec{j}_t) = 0$, we have simply for the case of planar geometry:

$$-d(j_h)/dx - \rho_h/\tau = 0 , \qquad (10)$$

where

$$j_h = -D_h d\rho_h/dx + \mu_h(E - e/4\epsilon x^2)\rho_h \qquad (10a)$$

and

$$-d(j_t)/dx + \rho_h/\tau = 0 , \qquad (11)$$

where

$$j_t = -D_t d\rho_t/dx + \mu_t(E - e/4\epsilon x^2)\rho_t . \qquad (11a)$$

In these equations D is the diffusion constant, μ is the mobility, and ϵ is the dielectric constant of the medium which we shall set equal to 1. Since Eq. (10) is decoupled from the thermal component we can find its solution independently. One boundary condition we shall use is

$$j_h(\infty) = 0 . \qquad (12)$$

Integrating Eq. (10) from x to ∞ and using (12) gives

$$j_h(x) = \tau^{-1}\int_x^\infty \rho_h(x)\, dx . \qquad (13)$$

Another boundary condition is given by the current balance at a distance of one mean free path from the cathode. One part of the electron current injected is scattered back without appreciable energy loss and another part diffuses into the medium. From Eq. (13) the latter part is given by $\int_\lambda^\infty \tau^{-1}\rho_h(x)dx$. The back scattered part can be written as $(1 - r)\rho_h(\lambda)\langle -v_x(\lambda)\rangle$ where r is the reflection coefficient at the cathode and $\langle -v_x(\lambda)\rangle$ is the average over all angles of the negative x component of the velocity at λ in the presence of the applied and image fields. If we define $\langle -v_x(\lambda)\rangle \equiv c(\lambda)\bar{v}_0$, where $\bar{v}_0$ is the average emission velocity; then $c(\lambda)$ must approach the Thomson value of 1/4 when λ is approximately x_M. The details of the calculation of

$c(\lambda)$ are shown in Appendix A. The current balance at λ can now be written as

$$j_0 = c'(\lambda)\rho_h(\lambda)\bar{v}_0 + \tau^{-1}\int_\lambda^\infty \rho_h(x)\,dx\,, \tag{14}$$

where

$$c'(\lambda) \equiv (1-r)c(\lambda)\,.$$

We now solve Eq. (11a) for ρ_t. From the continuity of current condition the measured current $j = j_h(x) + j_t(x)$. Substituting into Eq. (11a) $j - j_h(x)$ for $j_t(x)$ and $-dV/dx$ for the total field we get

$$j - j_h(x) = -D_t d\rho_t/dx - \mu_t(dV/dx)\rho_t\,.$$

Solving this equation for ρ_t we get

$$\rho_t(x) = \exp-[(\mu_t/D_t)V(x)]\int_0^x \{[j_h(x') - j]/D_t\} \times \exp[(\mu_t/D_t)V(x')]\,dx' + \rho_t(0)\,. \tag{15}$$

As $x \to \infty$ we don't expect ρ_t to diverge, but since $V(x) \to -\infty$, we must require that the integral in Eq. (15) vanishes. Thus we obtain

$$j = \frac{\int_0^\infty j_h(x)\exp[eV(x)/kT]\,dx}{\int_0^\infty \exp[eV(x)/kT]\,dx}\,, \tag{16}$$

where we have made use of the Einstein relation $\mu_t/D_t = e/kT$.

We now discuss the derivation of $\rho_h(x)$ from which $j_h(x)$, and hence j, can be calculated using Eqs. (13) and (16). Substituting Eq. (10a) into Eq. (10), we get

$$D_h\frac{d^2\rho_h}{dx^2} - \mu_h\left(E - \frac{e}{4\epsilon x^2}\right)\frac{d\rho_h}{dx} - \left(\frac{\mu_h e}{2\epsilon x^3} + \frac{1}{\tau}\right)\rho_h = 0\,. \tag{17}$$

Equation (17) can be solved by numerical methods. Typical solutions are shown in Fig. 3. Here we shall present a simple approximate solution and discuss its validity. We note that if the terms in Eq. (17) arising from the image field can be neglected, then the remaining equation can be solved analytically. We expect that the approximation might be justified for x above a certain distance x_{SD} for which $-D_h d\rho_h/dx \gg \mu_h(e/4\epsilon x^2)\rho_h$, and we call this the strong diffusion approximation (SDA). Estimates of x_{SD} are given in detail in Appendix B. The SDA solution to Eq. (17) is simply

$$\rho_h(x) = \rho_h(\lambda)\,e^{-\gamma(x-\lambda)}\,, \tag{18}$$

where

$$\gamma \equiv -\mu_h E/2D_h + [(\mu_h E/2D_h)^2 + x_0^{-2}]^{1/2} \tag{19}$$

and

$$x_0^2 = D_h\tau\,. \tag{20}$$

Applying the boundary condition (14), and $D_h = \frac{1}{3}\lambda\bar{v}_0$, we find

$$\rho_h(\lambda) = (j_0/\bar{v}_0)[c'(\lambda) + \lambda/3\gamma x_0^2]^{-1}\,. \tag{21}$$

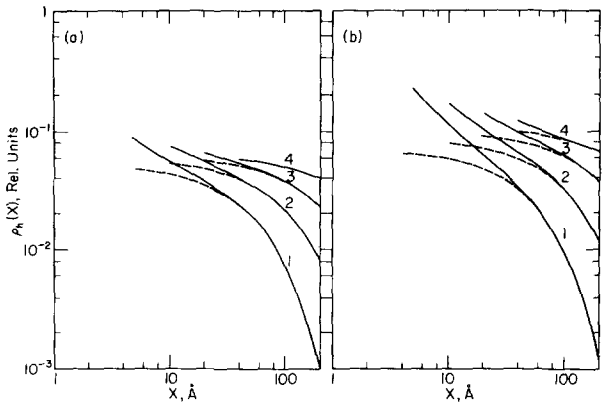

FIG. 3. Distribution of hot electrons obtained from the numerical solution to Eq. (17) (solid line) and from the strong diffusion approximation (broken line) for different electron m.f.p.: (1) 5 Å, (2) 10 Å, (3) 20 Å, (4) 40 Å, and for the energy of injected electrons (a) 1 eV; (b) 0.3 eV.

The comparisons of the SDA solution with the exact solution are shown in Fig. 3. It is observed that the deviation is greater for electrons of lower energy and shorter mean free path. This deviation is to be expected since under these conditions the diffusing electrons are more exposed to the influence of the image field. Their random velocity also becomes more sensitive to the change in the potential energy and the electrons undergo more scattering events closer to the emitter where the retarding field is high.

We can now calculate the SDA expression for the current by substituting Eq. (18) into Eq. (13) and then making use of Eq. (16), we get

$$Y = \frac{j}{j_0} = \frac{1}{1 + c'\bar{v}_0\gamma\tau}\,\frac{\int_0^\infty \exp(-\gamma x)\exp[eV(x)/kT]\,dx}{\int_0^\infty \exp[eV(x)/kT]\,dx}\,. \tag{22}$$

The first factor $(1 + c'\bar{v}_0\gamma\tau)^{-1}$ represents the fraction of the total current emitted from the source which is actually being injected into the medium. To illustrate this we consider the condition (14) for the current balance at a distance of one mean free path from the cathode. Substituting Eq. (18) into (14), we get

$$j_0 = c'(\lambda)\rho_h(\lambda)\bar{v}_0 + \rho_h(\lambda)/\gamma\tau = [1 + c'(\lambda)\bar{v}_0\gamma\tau]\rho_h(\lambda)/\gamma\tau\,.$$

Thus the fraction of electrons entering the medium is

$$\rho_h(\lambda)/\gamma\tau j_0 = 1/[1 + c'(\lambda)\bar{v}_0\gamma\tau]\,.$$

The second factor in Eq. (22) gives the collected fraction of the hot electron current that actually was emitted into the medium. Note that the fraction under the integral resembles the Onsager relation[15] for an exponential distribution of source currents. The meaning of this factor is illustrated

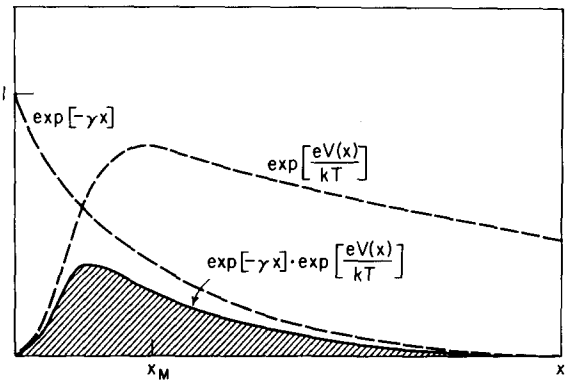

FIG. 4. The illustration of the effect of the image barrier on the yield in the electron injection experiments. The measured current is proportional to the area under the $\exp(-\gamma x)\exp[eV(x)/kT]$ curve where $V(x) = -Ex - e/4\epsilon x$. For slower thermalization, i.e. smaller γ, a greater fraction of the injected current is being collected since fewer electrons are thermalized in front of the barrier.

in Fig. 4. In the limit of very large fields, the factor becomes unity and Eq. (22) reduces to

$$Y = 1/[1 + c'(\lambda)\bar{v}_0\gamma\tau] .$$

Multiplying and dividing the right hand side of this equation by $\rho_h(\lambda)/\gamma\tau = j_2$ we get

$$Y = j_2/[j_2 + c'(\lambda)\rho_h(\lambda)\bar{v}_0] . \qquad (23)$$

Equation (23) is simply the expression derived by Bekiarian[9] if $c(\lambda)$ is taken to be $\frac{1}{4}$. The equation predicts that the yield is independent of the inelastic processes in the high field limit. This result is to be expected since most electrons are relaxing beyond the potential maximum for very high fields.

According to Eq. (22) the change in the thermalization distance, γ^{-1}, affects both the backscattering process and the yield of thermalized electrons. Fast energy relaxation decreases the importance of the backscattered hot electron current, since the first factor in Eq. (22) increases, but the fraction of collected electrons drops because more electrons are thermalized in front of the image barrier. The relationship between backscattering and the thermalization distance can be easily seen by considering the zero applied electric field case, then $\gamma^{-1} = x_0 = (\lambda\bar{v}_0\tau/3)^{1/2}$. The first factor in Eq. (22) becomes $(1 + c'\bar{v}_0\gamma\tau)^{-1} = (1 + 3c'x_0/\lambda)^{-1}$, where x_0 is the distance from the emitter where electron is thermalized.

III. EXPERIMENTAL RESULTS AND DISCUSSIONS

A. Argon

Figure 5 shows our experimental results for the yield versus the E/N ratio for several densities. At each density the log Y vs the log E/N curve (at each density the applied field is changed in order to vary E/N) is approximately a straight line of slope $\frac{1}{2}$ in the region where the Young and Bradbury validity condition $E/N > 0.01\sigma_p$ is satisfied. The results actually show that the range of validity can be extended to lower values of E/N. We have used the Young and Bradbury formula (7) to determine σ_p at each density N, the results are shown in Fig. 6. At low densities there is no dependence of σ_p on N and a value of about 7×10^{-16} cm^2 is obtained. This value is in reasonable agreement with those derived from other experiments.[16] At densities above 5×10^{21} cm^{-3} up to the liquid argon density, σ_p monotonically decreases with increasing density. It is of some interest to mention that the density range where σ_p deviates from the low density value coincides with that where argon deviates from the ideal gas behavior (Fig. 7). The possibility of the existence of a density dependent electron scatter-

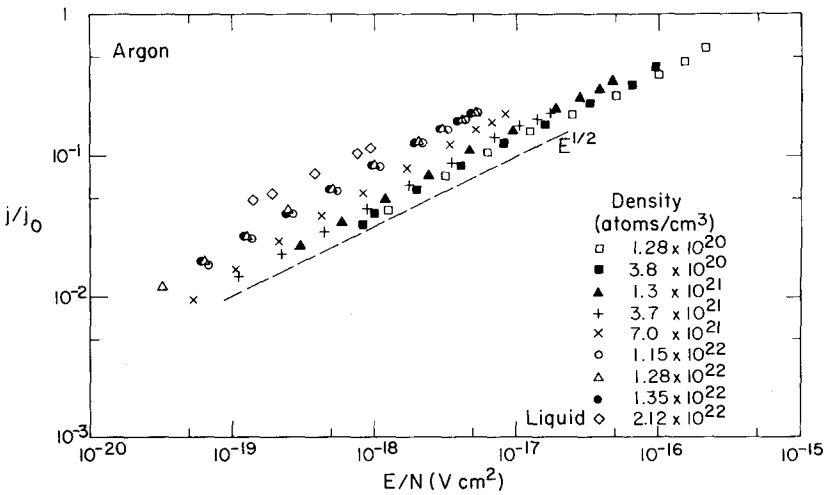

FIG. 5. The ratio of the measured current j to the current emitted into vacuum j_0 in argon gas at 160 °K and argon liquid at 87 °K as a function of the applied electric field E and the density N.

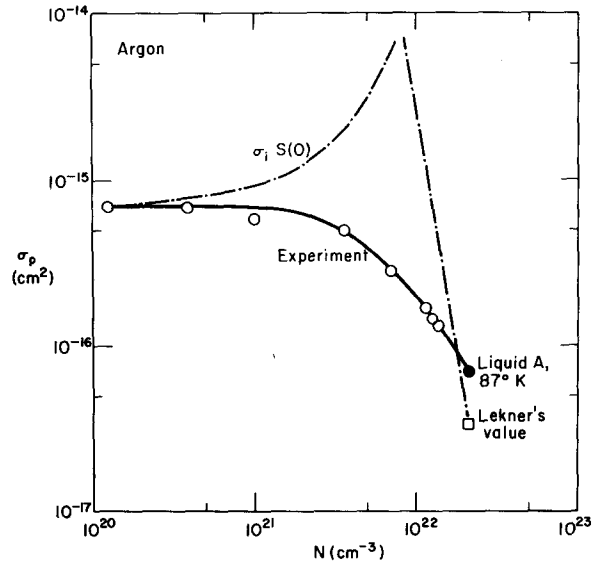

FIG. 6. Momentum exchange scattering cross section of hot electrons in argon as a function of density as derived from our experimental data using the Young and Bradbury model.

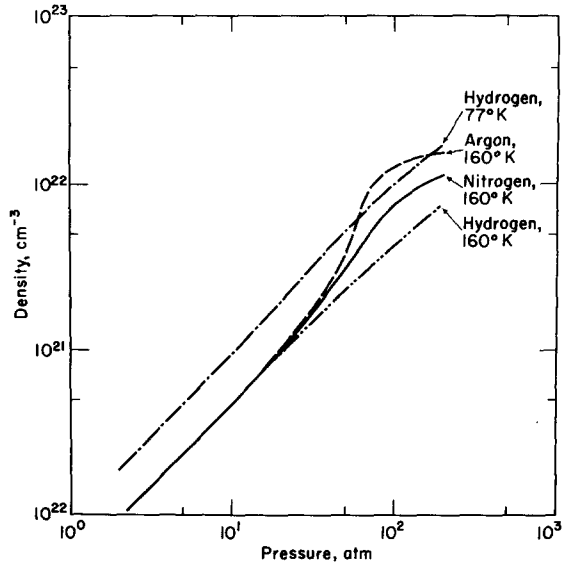

FIG. 7. Density of argon, nitrogen, and hydrogen vs gas pressure.

ing cross section in argon has been explored by Grünberg[17] and by Allen and Prew[18] who measured the electron drift velocity at different gas pressures. Neither group have detected any density dependence in the σ_p, apparently because the highest densities they reached were only about 1×10^{21} and 2.5×10^{21} cm^{-3}. Their results do not conflict with ours since the density effect becomes significant only above 5×10^{21} cm^{-3}.

From the Lekner's theory[19] of electron transport in liquid argon it follows that the momentum exchange cross section is

$$\sigma_p = \sigma_i S(0)\,, \tag{24}$$

where σ_i is the energy exchange scattering cross section and $S(0)$ is the Fourier transform of the two particle correlation function at zero momentum transfer. In this low momentum transfer limit

$$S(0) \simeq NkTX_t\,, \tag{25}$$

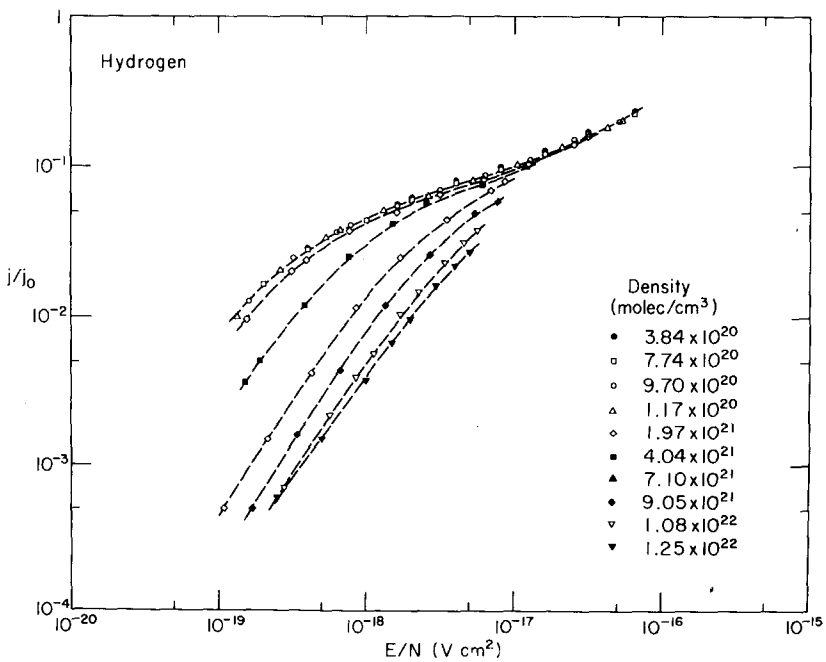

FIG. 8. The ratio of the measured current j to the current emitted into vacuum j_0 in hydrogen gas at 77 °K as as a function of the applied electric field E and the density N.

where X is the isothermal compressibility.

In Fig. 6 we also compare our experimentally derived values for σ_p with those obtained from Eqs. (24) and (25) using $S(0)$ values derived from thermodynamic data for argon.[20] As can be seen our results do not agree with this simple picture. This is not surprising because we have assumed that σ_i is independent of density. As Lekner has shown and from the experimental and theoretical analyses of Jahnke, Meyer, and Rice[21] σ_i should also depend upon density. Our results do not show the minimum in σ_p derived by Jahnke from his zero field mobility measurements. This also might be expected since Jahnke was observing thermalized electrons while we are looking at a swarm of electrons of 1 eV average energy. Jahnke noted that his mobility maxima tended to decrease in magnitude at higher field strengths where the electrons were hot. Drift experiments should be tried at field strengths which produce an average energy of 1 eV to compare with our injection results. We are presently planning such experiments.

B. Hydrogen and Nitrogen

Figure 8 shows the experimental results of H_2 and Fig. 9 shows the results for N_2. As can be seen in both sets of results, density has a marked effect on the magnitude of the observed current. This is particularly noticeable at high density and is due to thermalization at distances less than the maximum of the image potential. Equation (22) is used to analyze the data in Fig. 8 and Fig. 9. From the fit (solid lines) to these data we derive the values of the cross section σ_p and the relaxation time τ. The results are shown in Fig. 10. To obtain these results we assumed that r, the reflection coefficient, is zero since this gives values of σ_p at low densities which agree reasonably well with published data.[22] In their experiments, Bekiarian, Delcroix, and Ricateau,[9] found a large reflection coefficient. The difference between their results and ours are probably related to the facts that the electrodes used are different and prepared differently, our experiments are made at a much lower temperature (160 and 77 °K versus 300 °K) so that the layers of absorbed gas would be different. Also Bekiarian *et al.* did not take into account the effect of the field on $\langle -v_x(\lambda)\rangle$ which at high E/N will give an apparent large reflection coefficient. Since the conditions at the surface of the electrodes are difficult to determine anyway, it is not possible to ascribe more physical meaning to r at present except to treat it as an adjustable parameter as mentioned.

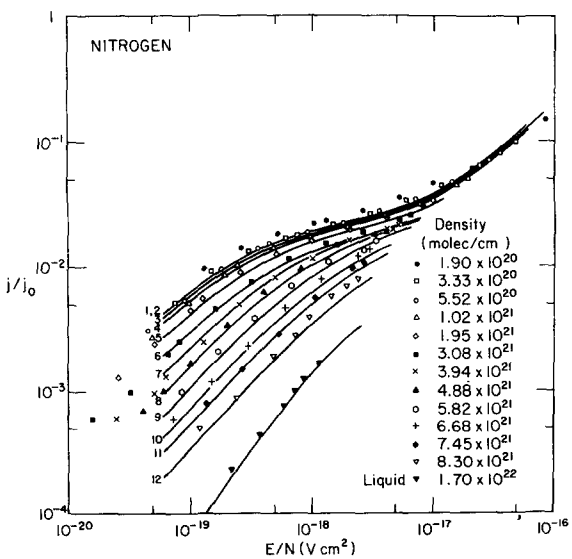

FIG. 9. The ratio of the measured current j to the current emitted into vacuum j_0 in nitrogen gas at 160 °K and nitrogen liquid at 77 °K as a function of the applied electric field E and the density N. The solid line shows the fit of Eq. (22). In order to obtain the agreement shown, it was necessary to make the thermalization time and the cross section density dependent. These dependences are given in Fig. 10.

The analysis of our data based on Eq. (22) is subject to the approximation of the SDA assumption. As mentioned earlier, a better solution to the continuity of current equation can be obtained numerically. It is of interest to estimate the error in the electron mean free path and hot electron lifetime if one uses the SDA solution. The estimates are presented in detail in Appendix C. We find that the SDA model underestimates electron mean free path and overestimates lifetime. For electron energy around 1 eV the error is quite small, however, for electron energy below 0.1 eV and electron mean free path of the order of 10 Å the error may exceed a factor of 2. In an experiment, the electrons are usually injected with a certain energy distribution. In Appendix D, the dependence of the measured mean free path and lifetime on the energy distribution of the injected electrons is discussed. The studied distributions of injected electrons are (a) monoenergetic, (b) photoelectric, and (c) thermionic. The thermionic distribution is of special interest since a larger amount of the emitted electrons have lower energies. Because of this feature the SDA assumption indicates in this case a greater error than the other two distributions. For the average injection energy of 1 eV and 20 Å mean free path the error is about 30% for the thermionic, about 18% for the photoelectric and 15% for the monoenergetic distribution.

Figure 10 shows that the momentum exchange scattering cross section, σ_p, for H_2 is essentially density independent. In the case of N_2, an increase in cross section was found at densities above

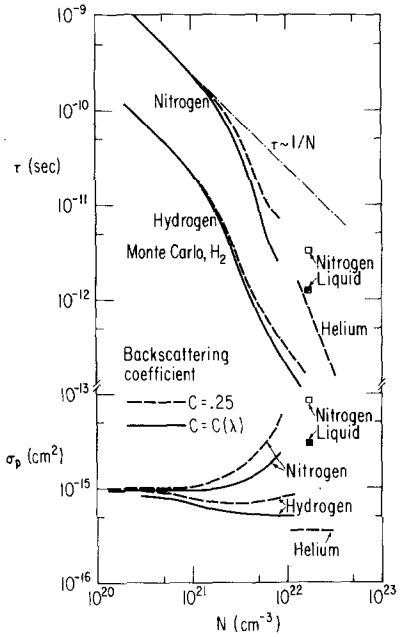

FIG. 10. The thermalization time τ and the momentum exchange scattering cross section σ_p of hot electrons in nitrogen, hydrogen, and helium as a function of density. The result for helium are taken from reference D. G. Onn and M. Silver, Phys. Rev A 3, 1773 (1971), and are shown for comparison.

3×10^{21} cm^{-3}. This density range also corresponds to that where thermodynamic data indicate a marked deviation from the ideal gas behavior (Fig. 7). In order to check that the effect didn't arise from approximation made in the reflection coefficient r and the return current $c'(\lambda)\rho_h(\lambda)\bar{v}_0$, we show in Fig. 10 the results of σ_p when two values of c', $c'=0.25$ (dashed curve) and $c'=c(\lambda)$ (solid curve), are used. If a finite reflection coefficients were used, c' will be less than $c(\lambda)$ and the two curves indicates that the density dependence of σ_p would have been stronger. The approximation introduced by using the SDA solution would not alter our conclusion either because our estimate in Appendix C and D shows that over the high density range involved, the approximation would cause an error no larger than about 40% while the increase in σ_p in this range is more than a 100%.

The high density variations in the cross sections in H_2 and N_2 are not understood. Drift experiments have also shown strong density dependence of scattering parameters at high densities. For example, electron drift velocity measurements in N_2 and H_2 indicate that the mobility decreases faster with density than $1/N$, and also that this effect is sensitive to the electron kinetic energy.[17,23] Allen and Prew,[18] e.g., did not detect any significant density dependence of electron mobility in N_2 at 1.7×10^{21} mole/cm^3 presumably because they had to work at high electric fields, ($E/N>10^{-17}$ cm^2). Frommhold[24] noted that the density dependence of the electron drift velocity in N_2 was consistent with the possibility of the existence of resonant scattering. According to his model the electron mobility is trap modulated, $\mu\sim(1+\nu\tau)^{-1}$, where τ is the lifetime of the resonant state, independent of density, and ν, the collision frequency, proportional to N. Legler[25] introduced multiple scattering as another mechanism giving a density dependent cross section. Bartels[26] tested both these models on his electron drift velocity data in H_2 and came to the conclusion that at low energies (< 25 meV), the density dependence of the drift velocity is in agreement with predictions of Legler's multiple scattering model[25] and at higher energies with the trapping model. In our experiment the average electron energy is about 1 eV, and, therefore, our data on electron scattering supplement those obtained from the drift velocity measurements.

Several possibilities exist for the increase of the scattering cross section found in N_2. One is the contributions from incoherent scatterings similar to those described by Davis.[27] Another is the existence of clusters[28] whose concentration might be significant at densities close to 10^{22} molecules/cm^3. Perhaps the contribution from clusters to the effective scattering cross sections may be evaluated from the temperature dependence. Another possibility is that the scattering length of the nitrogen molecule changes with density because of the changes in the effective potential at each molecule due to the closer proximity of nearest neighbors at higher densities. A calculation for N_2 similar to that performed by Lekner[19] for argon would be very helpful in clarifying this point. Density fluctuations and the possibility of "bubbles" in N_2 also can play an important part.[29]

Why the thermalization time decreases faster than $1/N$ in both N_2 and H_2 is also an open question. Perhaps as the density increases new vibrational and rotational deexcitation modes are opened up either due to clustering or some other many-body effects. Harrison and Springett[4] investigated the electron mobility vs density in dense H_2 at temperature between 26 and 32 °K. They have found evidence for the coexistence of two electron states, a quasi-free state and a low mobility state. Their data are similar to that found in dense helium where electrons are trapped in "bubbles" or "pseudobubbles."[30] It is certainly interesting that our results for τ in H_2 starts to decrease more rapidly than $1/N$ just at the same density where Harrison and Springett found "bubbles." If this correspondence can be carried over to N_2, then one should find bubbles above a density of 10^{21} cm^{-3} in N_2. In any

case, the density dependence of the lifetime and scattering cross section indicate that a simple free electron picture for the electronic states in these molecular substances is inadequate.

APPENDIX A

In order to calculate the rate of back scattered electrons, Thomson assumed that only those electrons at a distance of one mean free path from the electrode were collected. Further he assumed that because of scattering the angular distribution of these electrons was isotropic. In the absence of any electric field, the time of flight of an electron scattered at an angle θ with the $-x$ axis is $\lambda/\bar{v}_0\cos\theta$. The average negative x component of the velocity is given by

$$\langle -v_x\rangle = \frac{\bar{v}_0 \int_0^{\pi/2} \cos\theta \sin\theta \, d\theta}{\int_0^{\pi} \sin\theta \, d\theta} \quad . \tag{A1}$$

In our calculations we have included the effect of the image and the applied field upon the magnitude and direction of the velocity of the electrons as it goes from λ to the electrode. From simple energy conservation

$$v_x(\lambda) = \bar{v}_0[1 + (e^2/4\epsilon\lambda\mathcal{E}_0) + eE\lambda/\mathcal{E}_0]^{1/2}\cos\theta \, , \tag{A2}$$

where $\mathcal{E}_0$ is the injection energy (see Fig. 1).

Now

$$-dx/dt = v_x(X) = \{v_x^2(\lambda) + \bar{v}_0^2(e^2/4\epsilon\mathcal{E}_0) \times [(1/x) - (1/\lambda)] + \bar{v}_0^2 eE/\mathcal{E}_0(x-\lambda)\}^{1/2} \tag{A3}$$

from which we can calculate the time of flight which is

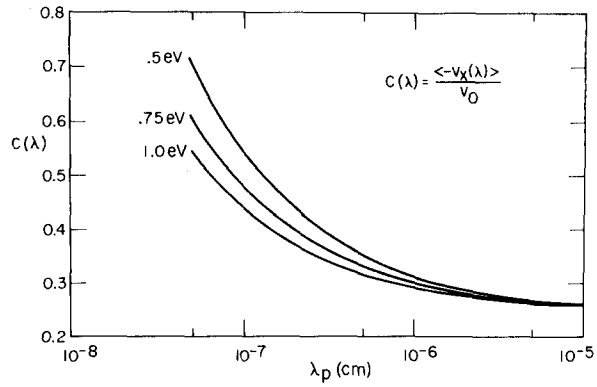

FIG. 11. Backscattering coefficient $c(\lambda)$ of hot electrons in the image field as calculated from Eq. (A4) and (A5) as a function of the electron mean free path λ and energy of injected electrons $\mathcal{E}_0$.

$$t(\theta) = \bar{v}_0^{-1} \int_0^{\lambda} \left\{ \left(1 + \frac{e^2}{4\epsilon\lambda\mathcal{E}_0}\right)\cos^2\theta + \frac{e^2}{4\epsilon\mathcal{E}_0}\left(\frac{1}{x} - \frac{1}{\lambda}\right) \right\}^{-1/2} dx. \tag{A4}$$

In Eq. (A4) we have neglected the small effect of the applied field. The average velocity then is

$$\langle -v_x(\lambda)\rangle = \frac{\lambda \int_0^{\pi/2} [\sin\theta \, d\theta/t(\theta)]}{\int_0^{\pi} \sin\theta \, d\theta} \quad . \tag{A5}$$

$c(\lambda)$ can be calculated by substituting (A4) into (A5), its values are shown in Fig. 11. For $\lambda \sim x_M$, $c(\lambda)$ approaches $\frac{1}{2}$ as expected. We have also neglected the electrons beyond $\theta = \pi/2$ which can be returned to the cathode because their path would be so long

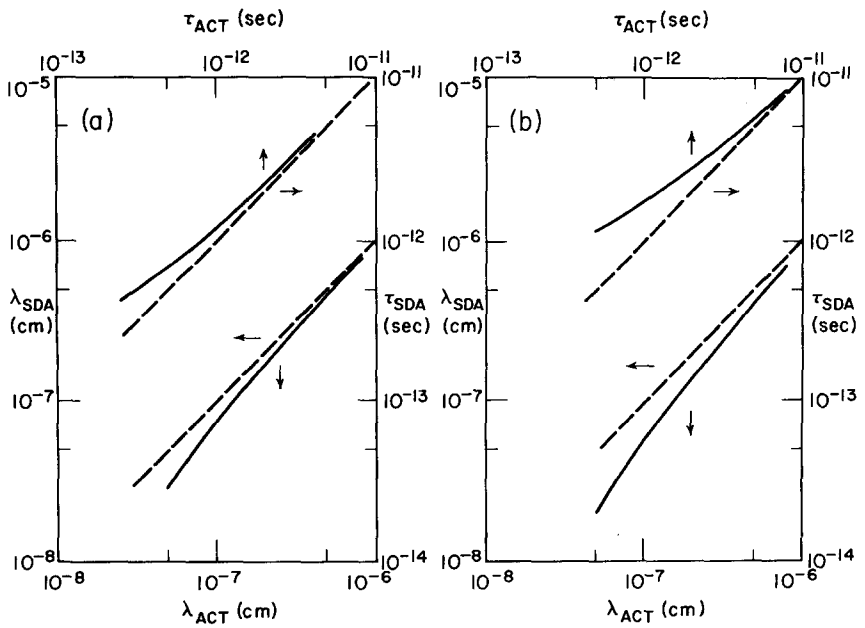

FIG. 12. Evaluation of errors produced by application of the strong diffusion approximation to the analysis of the measured current at $T = 0\,^{\circ}\mathrm{K}$. λ_{ACT} and τ_{ACT} are real values of the hot electron mean free path and lifetime. λ_{SDA} and τ_{SDA} are the corresponding quantities as determined from the strong diffusion approximation for energy of injected electrons (a) $\mathcal{E}_0 = 1$ eV, (b) $\mathcal{E}_0 = 0.3$ eV.

that they probably would encounter a second scattering event.

APPENDIX B

In order to estimate the value of x_{SD} such that for $x > x_{SD}$

$$-D_h \frac{d\rho_h}{dx} \gg \mu_h(e/4\epsilon x^2)\rho_h , \tag{A6}$$

we make the following approximations,

$$d\rho_h/dx \approx \rho_h/x_0 \tag{A7}$$

and

$$\mu_h/D_h \approx e/\langle \mathcal{E} \rangle , \tag{A8}$$

where $\langle \mathcal{E} \rangle$ is the average kinetic energy of the electrons, i.e., $\langle \mathcal{E} \rangle = \mathcal{E}_0 + e^2/4\epsilon x$. Substituting (A7) and (A8) into (A6) we find that the inequality (A6) is satisfied for

$$x > \frac{[1+(16\epsilon\mathcal{E}_0/e^2)x_0]^{1/2} - 1}{(8\epsilon\mathcal{E}_0/e^2)} . \tag{A9}$$

Assuming the thermalization distance $x_0 = 100$ Å, we find the critical distance x_{SD} to be 17 and 29 Å for 1 and 0.3 eV electrons, respectively. The curves in Fig. 3 shows that the SDA solution and the exact solution agree beyond a critical value of x slightly larger than that estimated here.

APPENDIX C

In order to estimate the error in the electron scattering mean free path and the hot electron lifetime derived from the SDA solution, we make the following gedanken experiment. We will inject monoenergetic electron current j_0 into a medium at $T = 0$ °K and measure the collected current which is determined by the value of the current at x_M. This current can be calculated by solving numerically Eq. (15) for assumed values of the actual hot electron mean free path λ_{ACT} and lifetime τ_{ACT}. We then analyze the same current using the SDA solution (22), and find λ_{SDA} and τ_{SDA}. The results are shown in Fig. 12 where two cases, (a) $\mathcal{E}_0 = 1$ eV and (b) $\mathcal{E}_0 = 0.3$ eV are shown. The mean free path and lifetime assumed are labeled λ_{ACT} and τ_{ACT} and those obtained from SDA approximation are λ_{SDA} and τ_{SDA}, respectively. As clearly shown the SDA underestimates λ and overestimates τ. The deviation is larger for lower injection energy and smaller mean free path.

APPENDIX D

In terms of the strong diffusion approximation at $T = 0$ °K, the measured current does not depend explicitly on the energy of the injected electrons. If the thermalization distance itself was energy independent, the energy distribution of electrons at the barrier maximum would be identical with the injected one. It would then be possible to correct for the effect of the energy distribution on the error in mean free path and lifetime by weighting each

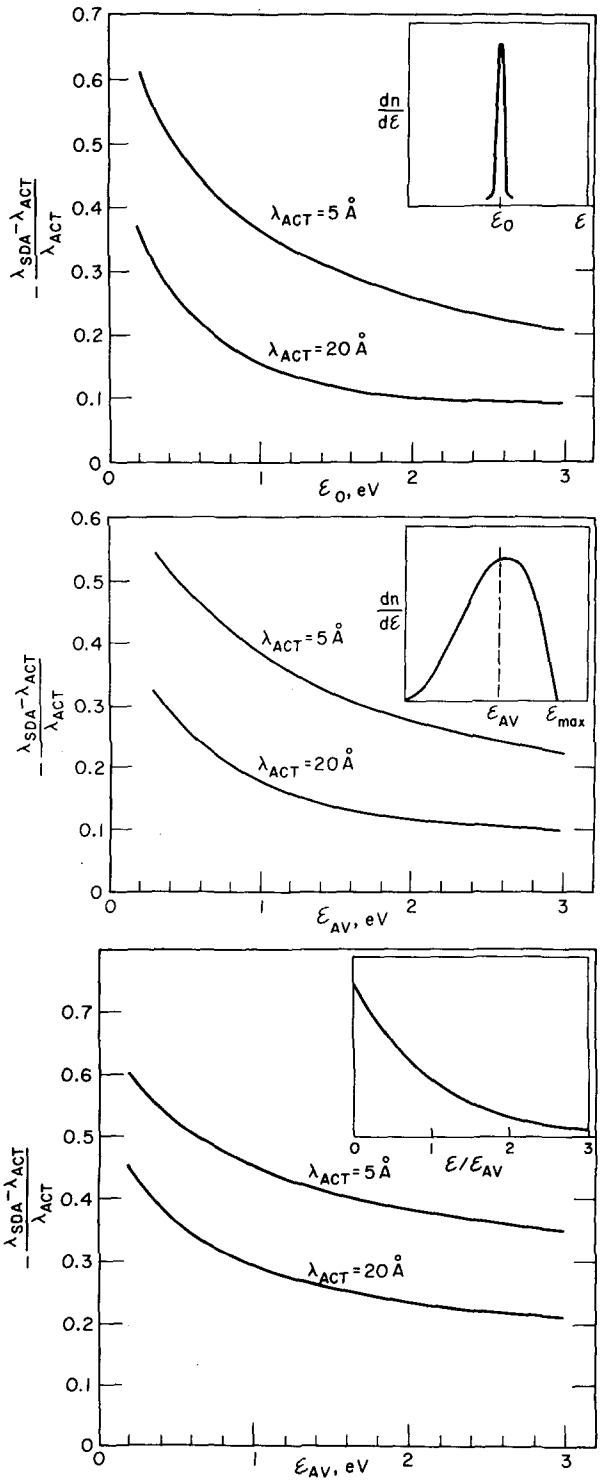

FIG. 13. Evaluation of errors produced by applying SDA method to the analysis of collected current when the distribution of injected electrons is (a) monoenergetic, (b) photoelectric, and (c) thermionic.

with the energy distribution function. However, the assumption of equal relaxation cross sections for electrons of different energies is not realistic since the inelastic scattering cross sections are energy dependent. It is rather more tractable to assign equal average lifetimes to all electrons. This way the relaxation distance becomes energy dependent according to the definition

$$x_0 \equiv [(2\mathcal{E}_0/m)^{1/2}(\lambda\tau/3)]^{1/2} \quad . \tag{A10}$$

In the constant lifetime approximation, the low energy electrons have shorter thermalization distance. The low energy electrons are more strongly attenuated, and therefore, their contribution to the measured current will be less. Another energy dependent effect comes in when we introduce the image potential. Figure 3 shows that the hot electron density decrease faster in the exact solution than in the SDA solution. Thus the image barrier also distorts the energy distribution of current at x_M. The two effects mentioned above were included in the estimate of errors produced by using the strong diffusion approximation. The error was estimated from the following procedure. For a selected value of the electron mean free path and for an assumed energy distribution of injected electrons, a numerical solution of the exact differential equation was sought. From the solution for each energy a contribution to the hot electron current is calculated using Eq. (13). The total current is then found by averaging over all incident energies $\mathcal{E}_0$ according to the energy distribution. For comparison we also analyzed the current by the SDA method where the energy distribution of injected electrons is replaced by a monoenergetic one with $\mathcal{E}_0$ equal to the average energy of the different distribution studied. The resulting discrepancies in λ are shown in Figs. 13(a), 13(b), and 13(c). In Fig. 13(a) the error derived from the exact solution and the SDA are shown for the monoenergetic case. The result will serve as a standard for evaluating the error in λ when the injection energy is not monoenergetic. In Fig. 13(b), the assumed distribution is photoelectric with $dn/d\mathcal{E} = (\pi/\mathcal{E}_{\max})^2 \mathcal{E} \sin(\pi\mathcal{E}/\mathcal{E}_{\max})$, where $\mathcal{E}_{\max} = \mathcal{E}_{av}\pi^2/(\pi^2-4)$. In Fig. 13(c), the distribution is thermionic with $dn/d\mathcal{E} = \exp(-\mathcal{E}/\mathcal{E}_{av})$.

*Work supported by the U. S. Army Research Office (Durham) and by the Advanced Research Projects Agency of the Department of Defense and monitored by the U. S. Army Research Office—Durham under Grant number DA-AROD-31-124-71-G52.

†Present address: Department of Physics, Portland State University, Portland, OR 97207.

[1](a)T. P. Eggarter and M. H. Cohen, Phys. Rev. Lett. **27,** 129 (1971). T. P. Eggarter, Phys. Rev. A **5,** 2496 (1972). J. P. Hernandez, Phys. Rev. A **5,** 635 (1972). (b)D. G. Onn and M. Silver, Phys. Rev. A **3,** 1773 (1971).
[2]L. S. Miller, S. Howe, and W. E. Spear, Phys. Rev. **166,** 871 (1968).
[3]B. Halpern and R. Gomer, J. Chem. Phys. **51,** 1031 (1969).
[4]H. R. Harrison and B. E. Springett, Chem. Phys. Lett. **10,** 418 (1970).
[5]C. R. Crowell and S. M. Sze, Phys. Thin Films **4,** 325 (1967). D. G. Onn, P. Smejtek and M. Silver, Proc. Intern. Conf. Low Temp. Phys. 13th Boulder, Co. 1972 (to be published).
[6]J. J. Thomson and G. P. Thomson, *Conduction of Electricity Through Gases* (Cambridge U. P., Cambridge, England, 1928), p. 466.
[7]J. K. Theobald, J. Appl. Phys. **24,** 123 (1953).
[8]L. B. Loeb, *Basic Processes of Gaseous Electronics* (University of California Press, Berkeley, CA, 1955), p. 604.
[9]A. Békiarian J. Phys. (Paris) **29,** 434 (1963), A. Békiarian, J. L. Delcroix, and P. Ricateau, C.R. Acad. Sci. (Paris) **265,** 238 (1967).
[10]T. Itoh and T. Musha, J. Phys. Soc. Jap. **15,** 1675 (1960).
[11]R. W. L. Thomas and W. R. L. Thomas, J. Phys. B 2, 562 (1969).
[12]J. Lucas, Int. J. Electron. **32,** 393 (1972).
[13]L. A. Young, and M. E. Bradbury, Phys. Rev. **43,** 34 (1933).
[14]Equation (6) is the same as Eq. (4) of Ref. 13.
[15]L. Onsager, Phys. Rev. **54,** 554 (1938).
[16]L. S. Frost and A. V. Phelps, Phys. Rev. **136,** 1538 (1964).
[17]R. Grunberg, Z. Naturforsch. A **23a,** 1994 (1968).
[18]N. L. Allen and B. A. Prew, J. Phys. B **3,** 1113 (1970).
[19]M. H. Cohen and J. Lekner, Phys. Rev. **158,** 305 (1967). J. Leknar, Phys. Rev. **158,** 130 (1967).
[20]A. L. Gosman, R. D. McCarty and J. G. Hust, *Thermodynamic Properties of Argon*, National Bureau of Standards 27; T. R. Strobridge, *The Thermodynamic Properties of Nitrogen* Nat. Bur. Stand., Technical Note 129; A. Michels, W. de Graaff, T. Wassenaar, J. M. H. Levelt, and P. Louwerse, Physica 25, 25 (1959).
[21]J. A. Jahnke, L. Meyer, and S. A. Rice, Phys. Rev. A **3,** 734 (1971).
[22]L. S. Frost and A. V. Phelps, Phys. Rev. **127,** 1621 (1962).
[23]J. J. Lowke, Aust. J. Phys. **16,** 115 (1963). R. W. Crompton, A. G. Robertson, Aust. J. Phys. **24,** J43 (1971).
[24]L. Frommhold, Phys. Rev. **172,** 118 (1968).
[25]W. Legler, Phys. Lett. A **31A,** 129 (1970).
[26]A. Bartels, Phys. Rev. Lett. **28,** 213 (1972).
[27]R. M. Minday, L. D. Schmidt, and H. T. Davis, J. Chem. Phys. **54,** 3112 (1971).
[28]T. A. Milne and F. T. Greene, J. Chem. Phys. **47,** 3668 (1967).
[29]J. P. Hernandez, Phys. Rev. A 7, 1755 (1973).
[30]J. A. Jahnke and M. Silver, Chem. Phys. Lett. 23, 231 (1973).